Beam heat load in the ANKA superconducting undulator

S. Casalbuoni*, A. Grau, M. Hagelstein, R. Rossmanith,
Forschungszentrum Karlsruhe, Karlsruhe, Germany
F. Zimmermann, CERN, Geneva, Switzerland,
B. Kostka, E. Mashkina, E. Steffens, University of Erlangen, Erlangen, Germany
A. Bernhard, D. Wollmann, T. Baumbach, University of Karlsruhe, Karlsruhe, Germany

Abstract

The beam heat load in the cold bore superconductive undulator installed at ANKA has been monitored for almost two years. The possible sources of the observed heat load as synchrotron radiation from upstream magnets, image currents, electron and ion bombardment are here discussed and compared with the experimental results.

INTRODUCTION

Conventional undulators are built with permanent magnets. The advantage of superconducting undulators is that for the same gap and same period length they produce higher fields. This technological solution is very interesting for synchrotron light sources since it permits to increase the brilliance [1, 2] at relatively low costs. Superconducting undulator technology has also recently been acknowledged by the high energy particle physics comunity to be the most promising solution for the CLIC damping wiggler [3] and for the ILC positron source [4]. However superconducting undulator technology is not yet mature. One of the key issues is the understanding of the beam heat load to the cold vacuum chamber. In this paper we present beam heat load measurements performed at the synchrotron light source ANKA in the superconducting cold bore undulator operating in the ring since March 2005.

EXPERIMENTAL SETUP

ANKA is an electron storage ring used as a synchrotron facility [5]. The maximum achievable energy is 2.5 GeV and the maximum current is 200 mA. The revolution time is $T_r = 368$ ns and the machine is normally operated with two trains, each composed of 32 bunches separated by 2 ns. The cold bore superconducting undulator built by ACCEL Instr. GmbH, Bergish, Gladbach, Germany [6], is installed in one of the four straight sections of the ring, see Fig. 1: the rest of the ring is warm. The vacuum chambers of the warm part of ANKA have been "prebaked ": before installation they have been baked at 200°C for 48 hours and vented with nitrogen. The storage ring compatible cryostat is shown in Fig. 2. The system is cryogen free and is cooled by three Sumitomo cryocoolers (RDK-408D @ 50 Hz) [7]: two of them are cooling the coils to about 4 K and one the UHV tank, which is at 10 K and protects the coils from the external thermal radiation. The cryostat consists of two separated vacuum systems for the cold mass: an UHV (Ultra High Vacuum) vacuum system for the beam and an insulation vacuum system for the coils and the rest of the cold mass. The pressure of the two vacua are monitored. A 300 μm stainless steel foil coated with 30 μm of copper is placed between the cold mass and the beam vacuum. A taper system connects the normal beam pipe with the cold mass and has two functions: 1) smooth transition for wake fields, 2) thermal transition between the cold bore at 4 K and the beam pipe at room temperature. Several temperature sensors are placed on the different elements: coils, UHV tank, taper entrance, taper exit, etc. The undulator can be operated at different gap sizes: 16, 12, and 8 mm. The undulator gap can be opened to 29 mm without current in the coils during injection. Some of the parameters of the electron beam, the storage ring and the superconducting undulator are summarized in Table 1. In order to protect the undulator from the synchrotron radiation emitted by the upstream magnets a collimator system is located at about 1 m from the entry point of the undulator [8].

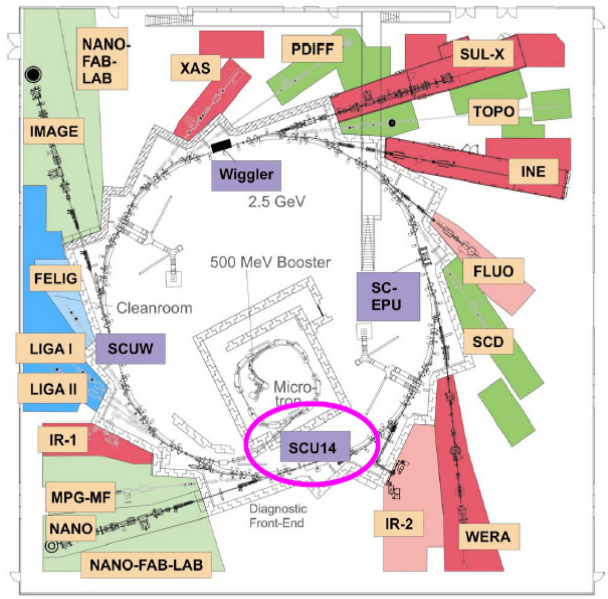

Figure 1: The synchrotron radiation facility ANKA.

POSSIBLE HEAT LOAD SOURCES

Possible heating mechanisms are: 1) synchrotron radiation from upstream magnets, 2) high frequency image currents on the cold surface also called resistive wall heating,

* sara.casalbuoni@iss.fzk.de

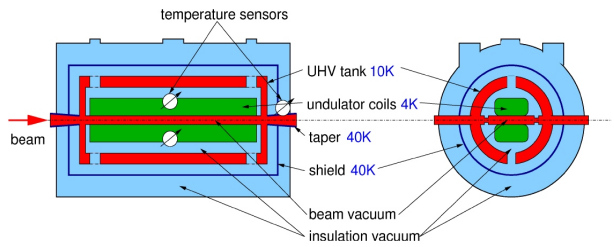

Figure 2: Schematic layout of the vacuum system of the superconducting undulator and the position of the temperature sensors.

Electron beam	
E_{max}	2.5 GeV
I_{max}	200 mA
Storage ring	
Circumference	110.4 m
Cavity frequency	499.66 MHz
T_{rev}	368 ns
Undulator	
Length	1.4 m
Periods	100
Magnetic gap	8,12, 16 mm
Beam stay clear gap	29 mm
Maximum magnetic field at 8 mm gap	0.8 T

Table 1: Electron beam, storage ring and superconducting undulator parameters.

3) ions and electrons accelerated to the walls by the transverse field of the ultrarelativistic beam. Knowing how the different heat load sources scale with the different beam parameters as the energy E, the average beam current I, the total number of bunches M, the bunch length σ_z and measuring the beam heat load varying the above mentioned parameters allows one to distinguish between the different heating mechanisms.

Heat load from synchrotron radiation

Synchrotron radiation losses are given by [9]:

$$P_{synch} = \int_{\psi_0}^{\psi_1} P_0 \frac{21}{32} \frac{\gamma}{(1+\gamma^2\psi^2)^{5/2}} \left[1 + \frac{5}{7} \frac{\gamma^2\psi^2}{(1+\gamma^2\psi^2)}\right] d\psi \quad (1)$$

where ψ is the vertical opening angle between the tangent of motion in the horizontal plane and the plane of interest, ψ_0 and ψ_1 are the lower and upper values of ψ determined by the distance of the bending magnet to the undulator and by the gap, $\gamma = E/m_e c^2$, $P_0 = \frac{eI}{10^3 6\pi\epsilon_0} \frac{E^4}{\rho(m_e c^4)^4}$ is the total radiated power per mrad of arc integrated over all vertical angles, e is the electron charge, I is the average beam current, ϵ_0 is the vacuum permittivity, E is the beam energy, ρ is the radius of curvature of the electron trajectory in the bending magnet, m_e is the electron mass and c is the velocity of light.

Heat load from resistive wall effect

The resistive wall heating losses per unit length can be calculated by [10]:

$$P_{RWH} = \frac{I^2}{M f_0 \pi^2 g} \int_0^\infty S^2(\omega) R_{surf}(\omega) d\omega \quad \text{[W/m]} \quad (2)$$

where I is the average beam current, M is the number of bunches, f_0 the revolution frequency and g is the gap (an equivalent formula is given in Ref. [9]). $S(\omega)$ is the bunch spectrum. Assuming a bunch with Gaussian shape and length σ_z, $S(\omega) = e^{-\frac{\sigma_z^2\omega^2}{2c^2}}$. $R_{surf}(\omega)$ is the surface resistance. The vacuum chamber is made of a 300 μm layer of stainless steel electroplated with 30 μm of copper. Electroplated copper has usually a Residual Resistivity Ratio (RRR) in the range between 10 and 100 [9]. For copper at low temperature and $RRR > 7$ we are in the regime of the anomalous skin effect [9, 10, 11] and:

$$R_{surf}(\omega) = R_\infty(\omega)(1 + 1.157\alpha^{-0.276}), \quad \text{for } \alpha \geq 3 \quad (3)$$

with $\alpha = \frac{3}{2}(\frac{\ell}{\delta(\omega)})^2 = \frac{3}{4}\mu_r\mu_0\sigma\omega\ell^2$ where ℓ is the mean free path, $\delta(\omega) = \sqrt{\frac{2}{\mu_r\mu_0\sigma\omega}}$ the skin depth, μ_r the relative permeability, μ_0 the vacuum permeability and σ the electrical conductivity, and with $R_\infty(\omega) = (\frac{\sqrt{3}}{16\pi}\frac{\ell}{\sigma}(\mu_r\mu_0\omega)^2)^{1/3}$.

Synchrotron radiation losses increase linearly with the average beam current, while resistive wall heating losses scale as I^2/M and strongly depend on the bunch length σ_z.

Heat load from electron and ion bombardment

A naive model of heat load due to electron and ion bombardment is described below. A charged particle with mass m and charge q in the vacuum chamber can be accelerated by the transverse electric field carried by the ultrarelativistic bunch:

$$E(r) = \frac{\lambda}{2\pi\epsilon_0 r} \quad (4)$$

where λ is the line charge of the bunch, $\lambda = \frac{eN_b}{c\tau}$ and τ is the bunch duration and N_b the particles per bunch $N_b = \frac{IT_r}{eM}$ with T_r the revolution time [12]. The momentum transfer by one bunch to a stationary electron at radial position r is

$$\Delta p = qE(r)\tau = \frac{qeN_b}{2\pi\epsilon_0 cr} \quad (5)$$

and the corresponding energy increase:

$$\Delta W = \frac{\Delta p^2}{2m} = \frac{\left(\frac{qeN_b}{2\pi\epsilon_0 cr}\right)^2}{2m}. \quad (6)$$

Roughly, the power is the energy gained by the charged particle ΔW times the number of charged particles accelerated to the wall per unit time $\dot{\Gamma}$:

$$P_{el} = \Delta W \cdot \dot{\Gamma} \quad (7)$$

Since the energy ΔW is inversely proportional to the mass of the particle m the ion contribution can be neglected, see Eq. (6). It is then known how the energy gain scales with the different beam parameters. A possible source of electrons is the condensed gas layer physisorbed on the surface. In the gas layer the molecules are loosely bound (binding energy $\approx$ few meV) by Van der Waals forces (see Fig. 3). The gas layer is formed at low temperatures. Energetic particles first hit the surface oxide layer of the vacuum chamber and part of the gases are desorbed. Then the desorbed gases recondense on the surface, so that the energetic particles will after hit the condensed gas layer where the molecules are loosely bound and this can be a source of electrons. Since the molecules forming the condensed gas layer have already been desorbed this phenomenon is usually refered in the literature as "recycling"(see for example Ref. [13]). Our vacuum chamber is very similar to the LHC beam screen (300 μm stainless steel with 30 μm of electroplated copper). For such a chamber the dominating desorbed gases are H_2, CH_4, CO, CO_2 and H_2O. Of these only H_2 has a non negligible vapour pressure at 4-20 K. The plot in Fig. 4 from Ref. [15] shows the adsorption isotherm of H_2 at 4.2 K, that is the density of H_2 molecules in gas form n, corresponding to the equilibrium pressure measured at room temperature $P_{UHV} = n(\text{mol/cm}^3) \cdot 4.9 \cdot 10^{-18}$ mbar [15] as a function of the H_2 surface coverage s. The adsorption isotherm varies with many parameters as the molecular species present in the surface oxide, on the surface temperature, on the nature of the surface oxide and on the gas composition inside the chamber. In the vacuum chamber of the superconducting undulator the equilibrium pressure is about $2 - 5 \cdot 10^{-11}$ mbar, which corresponds to 10^{15} H_2 molecules per cm^2. Considering the geometry of our vacuum chamber we can calculate the number of H_2 molecules on the surface and in the volume. At the surface we have $N_{Surf} \approx 10^{17}$ and in the volume, considering $P_{UHV} = 10^{-11}$ mbar, $N_{Vol} \approx 5 \cdot 10^{10}$. At the surface there are more than one milion times molecules than in the volume: the surface is a huge electron reservoir. The mass

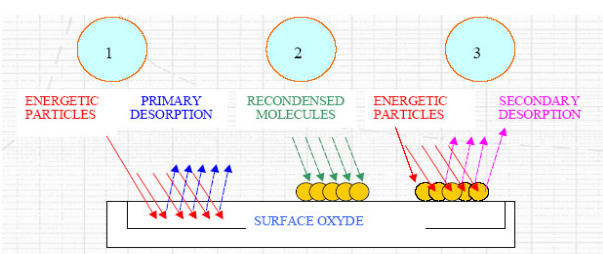

Figure 3: Scheme of the desorption process on a cold surface. After N. Hilleret [14].

spectrum of the warm vacuum chamber just before the undulator with beam detects only H_2 and CO, see Fig 5. CO disappears when there is no beam: this is an indication of the dynamic of the desorption and recycling process discussed above. In the rest of the ring most of the time no

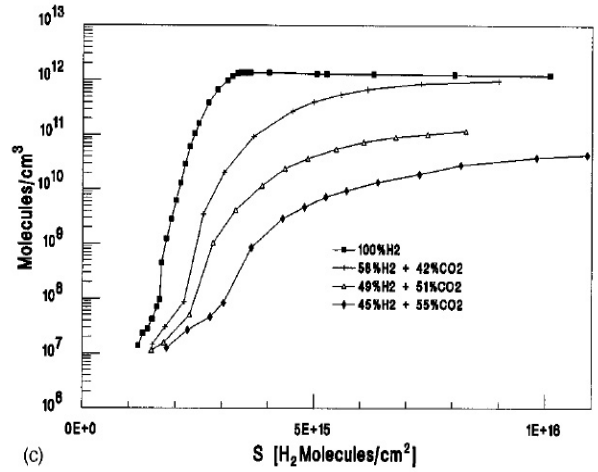

Figure 4: Isotherms of coadsorption of H_2 and CO_2 on Cu plated stainless steel at 4.2 K, plotted as a function of the surface density of H_2 molecules. After E. Wallén [15].

CO is detected.

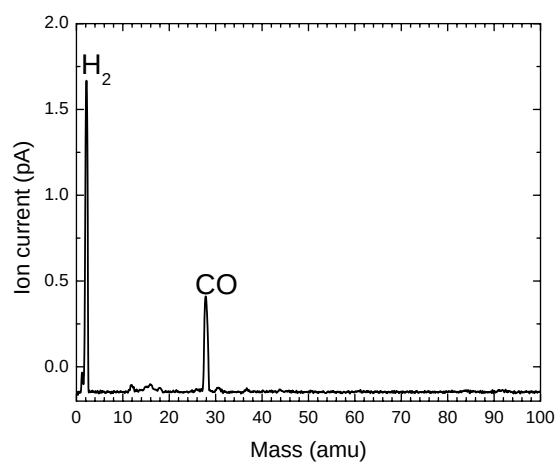

Figure 5: Mass spectrum of the warm vacuum chamber just before the undulator with beam.

RESULTS

Beam induced heat load during normal beam operation

Fig. 6 shows the average beam current, the beam energy, the UHV pressure and the temperature of the coils as a function of time during user operation in a time range of 2 weeks. The increase in temperature to the coils can be converted into the deposited beam heat load. The calibration has been performed using a resistor in thermal contact with the coils. The time constant to reach thermal equilibrium is of the order of two hours. The beam heat load to the coils is about 1 W. A pressure rise is observed after

injection. In Fig. 7 are reported the heat load (upper plot) and the pressure (lower plot) as a function of the beam current. The heat load is higher when the pressure is higher. A correlation between the heat load and the pressure is observed, (see inset of the upper plot). In the lower plot of Fig. 7 a non-linear increase in the pressure is observed by increasing the beam current. A maximum of the pressure is observed for an average current of about 160 mA. The peak shifts to lower currents of about 140 mA when the pressure is higher. A similar pressure rise with current has been observed in the positron ring at the Bfactory PEPII, a warm machine, for high currents and has been attributed to electron multipacting [16]. During the user operation mode of

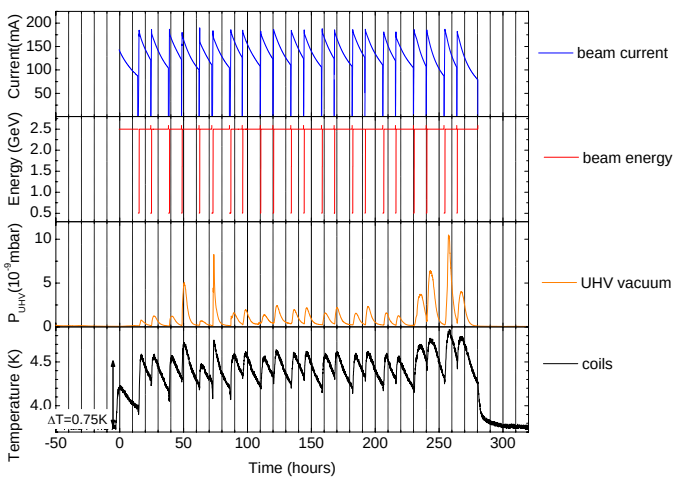

Figure 6: Typical user operation run with open gap (= 29 mm) and no current in the undulator. The beam current, the beam energy, the UHV pressure and the temperature of the coils are reported as a function of time.

ANKA a large variation of the heat load and of the UHV pressure is observed. In Fig. 8 is shown the heat load (upper plot) and the UHV pressure (lower plot) as a function of the average beam current I measured over half a year. In all cases the orbit is identical. The different colours refer to different runs over periods of about two weeks (similar to what is shown in Fig. 6 and in Fig. 7). The low current run measured during one of the machine shifts dedicated to the superconducting undulator studies indicates the correct calibration of the beam heat load: the heat load goes to zero for low beam currents. In the inset of the upper plot of Fig. 8 the beam heat load is shown as a function of the UHV pressure. A correlation between the two measured quantities is observed: above a certain heat load and pressure the heat load increases by increasing the pressure, below it is independent.

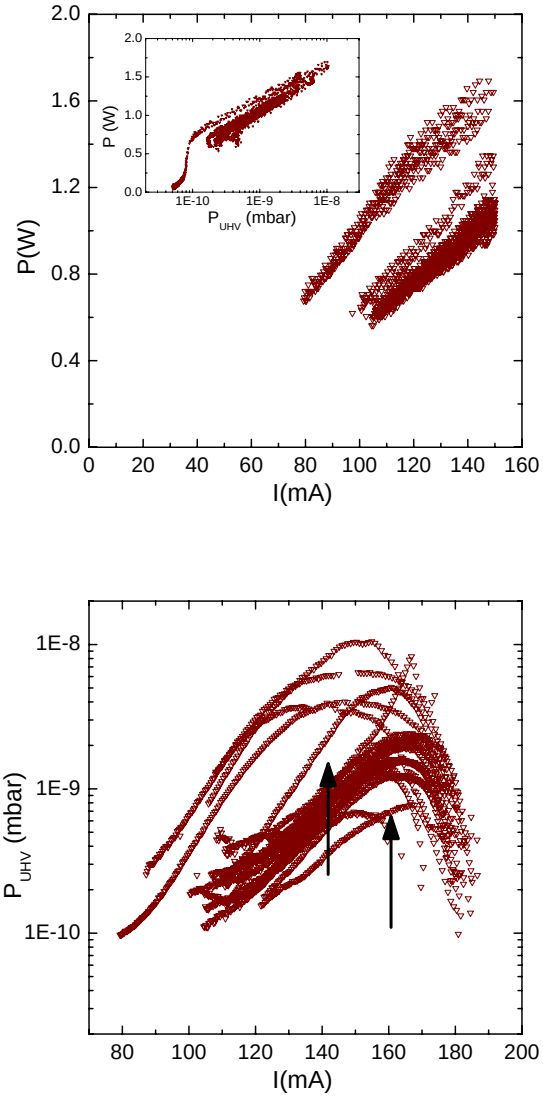

Figure 7: Upper plot: the beam heat load from Fig. 6 is shown as a function of the average beam current I and in the inset the beam heat load as a function of the UHV pressure. Lower plot: the UHV pressure from Fig. 6 is shown as a function of the average beam current I. The arrows indicate the current where the peak pressure is observed.

Dependence of the beam heat load on filling patterns

We have studied the dependence of the beam heat load as a function of current for different filling patterns. ANKA can be filled with one bunch train consisting of 32 bunches with a bunch spacing of 2 ns, or two or three bunch trains spaced by 120 ns. This allows to change the bunch current while the average current remains identical. Keeping in mind that for the following measurements less statistics is available, the beam heat load measured as a function of the

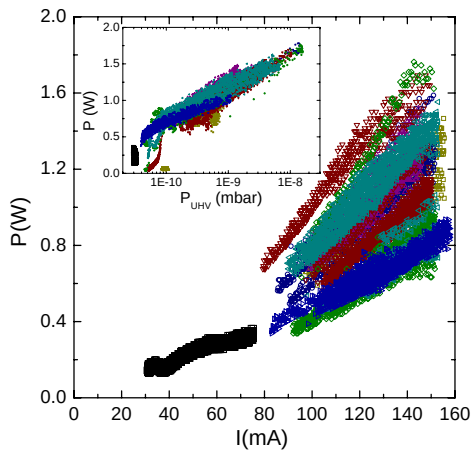

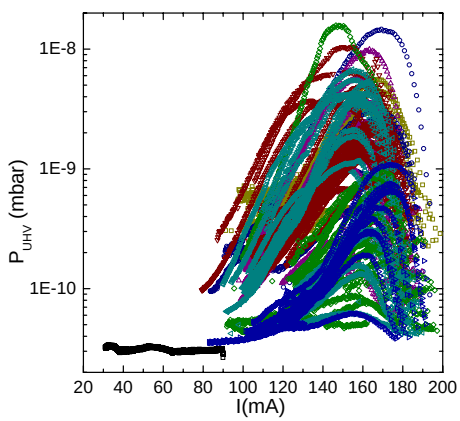

Figure 8: Variation over half a year of the beam heat load (upper plot) and of the UHV pressure (lower plot) reported as a function of the average beam current. The different colours refer to different runs over a period of about two weeks. In the inset of the left plot the beam heat load is shown as a function of the UHV pressure. Beam parameters: E=2.5 GeV, I=80-200 mA, two trains. Undulator parameters: gap= 29 mm, undulator current=0 A.

average beam current for 16 mm gap (see Fig. 9) scales as:

$$P \propto \frac{I^2}{M} \tag{8}$$

where I is the stored average beam current and M the total number of bunches per revolution. Such a scaling is typical for losses caused by resistive mechanisms.

In the inset of Fig. 9 the UHV pressure as a function of the average beam current is shown. The pressure rise is in some runs quite low and no peak is observed as a function of current. In case of electron bombardment a possible explanation would be the dependence of the peak current on the beam history: it is in fact known that the desorption coefficients and the secondary emission yields of the different gas molecules adsorbed on the vacuum chamber decrease with beam exposure time (electron dose) [13].

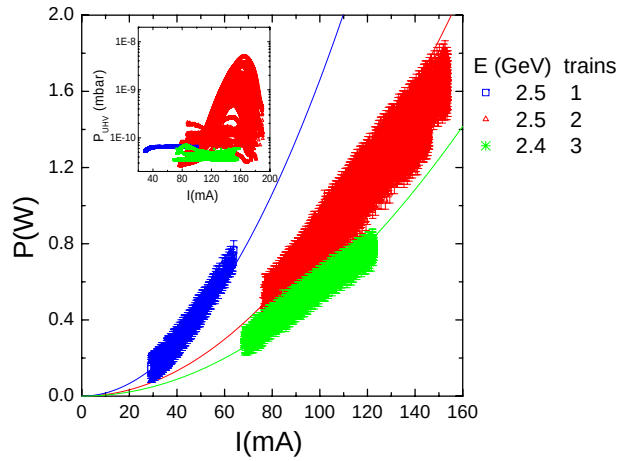

Figure 9: The beam heat load reported as a function of the average beam current for three different filling patterns. The three curves are polynomial fits demonstrating the scaling law $P \propto I^2/M$. Blue line: $P(\mathrm{W}) = 1.66 \times 10^{-4} I^2(\mathrm{mA})$. Red line: $P(\mathrm{W}) = 1.66/2 \times 10^{-4} I^2(\mathrm{mA})$. Green line: $P(\mathrm{W}) = 1.66/3 \times 10^{-4} I^2(\mathrm{mA})$. In the inset the UHV pressure is shown as a function of average beam current.

Beam heat load with sub-picosecond pulses

In order to produce short bunches of a few hundreds fs ANKA can be operated in the so-called low α mode [17]. The measured beam heat load for a run in the low α mode with one train at E=1.3GeV and a gap=29mm is shown in Fig. 10. The data can be well fitted by the resistive wall heating model using Eq. (2) taking into account the anomalous skin effect, assuming a RRR=100 and a bunch length of 500 fs. The value of 500 fs is consistent with the bunch lengths measured in the low α mode by means of THz edge synchrotron radiation [19]. During standard operation the bunch length varies with beam energy. The heat load induced by resistive wall effects should be higher at lower energies since the bunch length is shorter. This is not the case. So resistive wall heating seems to be dominant for short bunches but not for longer ones. We conclude that another heating mechanism must be responsible for the beam heat load observed during user operation.

Heat load by changing the gas content in the undulator

With the aim to see if the effect is caused by the gas composition, H_2 was injected in the warm side before and after the undulator. A scheme of the experimental setup is shown in Fig. 11. The idea is to increase the equilibrium pressure to enhance the H_2 surface coverage s and consequently the beam heat load. We were able to change the equilibrium pressure only by about a factor of 2.5 from $2 \cdot 10^{-11}$ mbar to $5 \cdot 10^{-11}$ mbar, so the surface coverage could not significantly be changed (see Fig. 4). The results

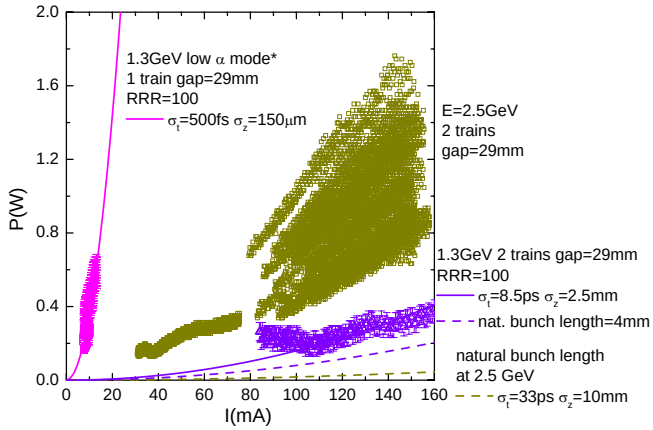

Figure 10: The beam heat load reported as a function of the average beam current for three different bunch lengths. The four curves are theoretical predictions based on Eq. (2) computed for different bunch legnths as indicated. The dashed curves are obtained with the natural bunch length (defined only for the normal optic of the ring, so for longer bunches), derived from Ref. [18]. The continuous curves are obtained by using bunch lengths values to fit the experimental data.

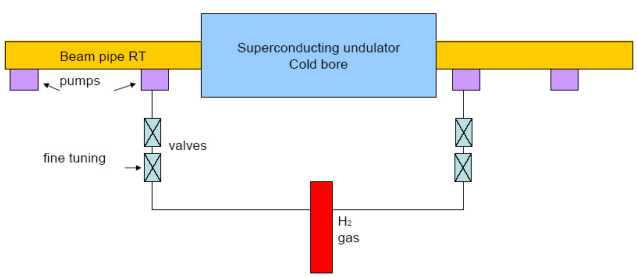

Figure 11: Scheme of the experimental setup for H_2 injection in the undulator.

are shown in Fig. 12: the beam heat load does not change. Two runs with respectively three and two trains have been performed. Figure 12 also shows two successive runs without further injecting H_2 and with pumps once on and once off. The pressure gets higher during all the runs and the current where the peak pressure is observed shifts to values lower than observed before H_2 injection (see the run with $E = 2.5$ GeV with two trains, open red triangles). As shown in the inset of the upper plot of Fig. 12, again a correlation is observed between the beam heat load and the pressure. We also observe (see lower plot of Fig. 12) that the current where the peak pressure is observed depends on the number of bunches: for two trains it is lower than for three trains.

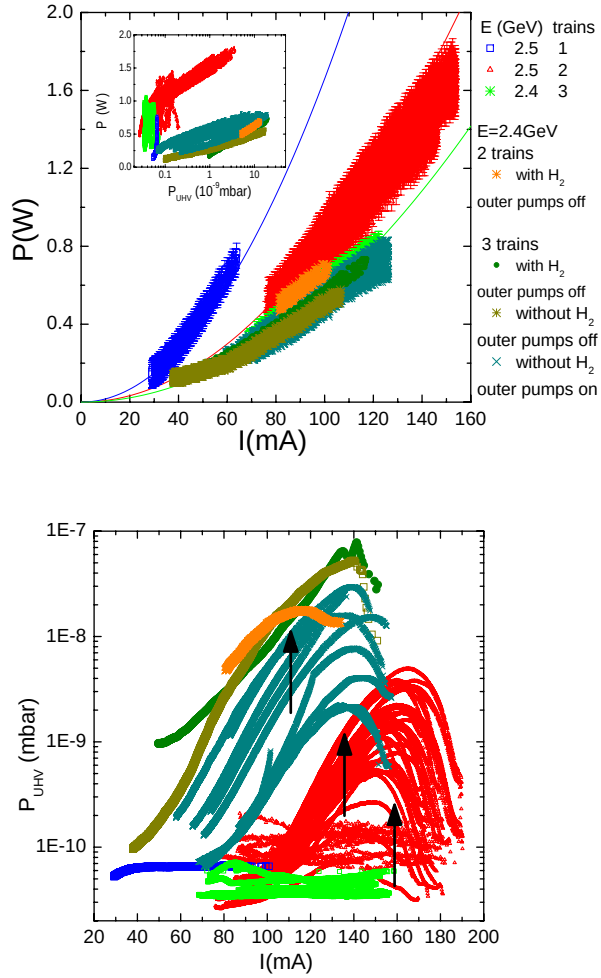

Figure 12: The beam heat load (upper plot) and the UHV pressure (lower plot) are shown as a function of the average beam current I. In the upper plot the three curves (continous lines) have been explained in Fig. 9. The arrows in the lower plot indicate the current at which the pressure has a peak. Starting from high currents they refer to: run with E=2.5 GeV, two trains and no H_2 injected (red open triangles), run with E=2.4 GeV, three trains, H_2 injected and after injection (olive green circles, dark yellow stars and dark cyan crosses), run with E=2.4 GeV, two trains and H_2 injected (orange stars). In the inset the beam heat load is reported as a function of the UHV pressure. The beam parameters and the undulator gap are indicated in the upper plot for the different runs. In all cases the current in the superconducting coils of the undulator is zero.

Pressure rise and heat load due to electron bombardement

The equations of gas dynamic balance inside a vacuum chamber can be written as (see Ref. [20, 21] and references

therein):

$$\begin{aligned} V\frac{dn}{dt} &= q + q'(s) - \alpha S(n - n_e(s,T)) + u\frac{d^2n}{dz^2}; \\ A\frac{ds}{dt} &= \alpha S(n - n_e(s,T)) - q'(s) \end{aligned} \quad (9)$$

where n is the volume gas density, s the surface density of the cryosorbed gas, V the vacuum chamber volume, A the vacuum chamber wall area, q is the primary beam induced desorption flux, q' the secondary beam induced desorption flux (desorption of cryosorbed molecules), α the sticking coefficient, $S = A\bar{\nu}/4$ is the ideal wall pumping speed, $\bar{\nu}$ is the mean molecular speed, n_e the thermal equilibrium gas density, and u the specific vacuum chamber conductance per unit axial length. The beam induced desorption flux consists of photon (PSD) and electron (ESD) stimulated desorption:

$$\begin{aligned} q &= \eta\dot{\Gamma} + \phi\dot{\Theta}; \\ q' &= \eta'\dot{\Gamma} + \phi'\dot{\Theta}; \end{aligned} \quad (10)$$

where η and η' are the primary and secondary electron stimulated desorption yields, $\dot{\Gamma}$ is the electron flux, ϕ and ϕ' are the primary and secondary photodesorption yields, and $\dot{\Theta}$ is the photon flux.

The volume gas density n at a temperature T is related to the pressure measured at room temperature by:

$$n = \frac{P}{k_B\sqrt{TT_{RT}}} \quad (11)$$

When the pressure reaches the maximum (see Fig. 6) as a function of time, $dn/dt = 0$. The u the specific vacuum chamber conductance per unit axial length is given by $u = A_c D$, where $D = 2/3A_c\bar{\nu}$ is the Knudsen diffusion coefficient being A_c the area of the rectangular cross section of the vacuum chamber. Axial diffusion can be neglected when $DA_c/L^2 < S\alpha$ [20], which means:

$$\frac{8}{3}\frac{A_c^2}{AL^2} < \alpha \quad (12)$$

Experimental values of the sticking coefficient for H_2 at 4.2 K indicate $\alpha > 0.02$ [22]. Even considering $\alpha = 0.02$ condition (12) is satisfied for the geometry of the undulator vacuum chamber where L=1.4 m and for a gap of 29 mm, $A_c = 0.00191$ m^2 and $A = 0.266$ m^2. Neglecting axial diffusion $ud^2n/dz^2 \approx 0$, the sum of the primary and recycling desorption yield of all gas species can be computed using the following equation:

$$\frac{q + q'}{\alpha} = S(n - n_e(s,T)) = SG\Delta P \quad (13)$$

where $\Delta P = P_{max} - P_e$ with $P_e \approx 2 \cdot 10^{-11}$ mbar the thermal equilibrium pressure and $G = \frac{1}{k_B\sqrt{TT_{RT}}} = 2 \cdot 10^{17}$ cm^{-3}/mbar. For the ANKA cold bore vacuum chamber with gap = 29 mm and average beam current $I = 100$ mA, the photon flux impinging on the lower and upper surfaces is $\dot{\Theta} \approx 10^{16}$ photons/s.

If the heat load observed is generated by electron bombardment and assuming a mean electron energy $\Delta W = 10$ eV, the estimated electron flux for a heat load of $P = 1$ W is $\dot{\Gamma} \approx 6 \cdot 10^{17}$ electrons/s. Being $\phi + \phi' \lesssim \eta + \eta'$ [13, 23], we can neglect the PSD to the beam desorption flux, so that $q = \eta\dot{\Gamma}$ and $q' = \eta'\dot{\Gamma}$. The observed ΔP ranges from $2 \cdot 10^{-11}$ mbar to $8 \cdot 10^{-8}$ mbar. For H_2 the mean molecular speed at 4.2 K is $\bar{\nu} = 210$ m/s. The area of the vacuum chamber for a gap=29 mm is $A = 0.266$ m^2. Applying Eq.(13) we find that the sum of the primary and secondary desorption yields for H_2 $(\eta + \eta')/\alpha$ ranges between 10^{-4} molecules/electron to 4 molecules/electron. Our values are in good agreement with the ones measured at COLDEX [13] that range between 10^{-2} molecules/electron for an electron dose of $2 \cdot 10^{19}$ electrons/cm^2 to 30 molecules/electron for an electron dose of 10^{17} electrons/cm^2, considering that in our case the temperature is lower (4.2 K instead of 12 K), the mean electron energy is an order of magnitude smaller (10 eV instead of 100 eV) and that our electron dose is in some cases much higher (after two weeks of normal user operation it is about $2 \cdot 10^{20}$ electrons/cm^2).

CONCLUSIONS AND OPEN QUESTIONS

A non-linear pressure rise with current is observed. This rise might be due to H_2 recycling and/or electron multipacting. The current where the peak pressure is observed is lower when the pressure is higher and it decreases also for higher bunch currents. The peak is not always observed. One possible explanation would be the dependence of the peak current on the beam history: it is in fact known that the desorption coefficients and the secondary emission yields of the different gas molecules adsorbed on the vacuum chamber decrease by increasing the beam exposure time [13].

Concerning the beam heat load we have compared the data with theoretical predictions from different models. Synchrotron radiation cannot explain the data since it predicts a linear dependence with current which is not observed. The resistive wall heating model can fit the data for short bunches but it does not for longer bunches. We do observe that the heat load scales with I^2/M, which is typical for resistive effects. On the other hand a smaller beam heat is observed at lower beam energies when the bunch length is shorter. Resistive effects would imply to observe a higher beam heat load for shorter bunches. Resistive effects also can not explain the large variation in the beam heat load.

The electron bombardment model is consistent with the beam heat load and pressure rise observed during normal user operation (longer bunches). Still to be understood is the mechanism responsible for releasing the electrons from the gas layer cryosorbed on the wall of the vacuum chamber.

ACKNOWLEDGEMENTS

The authors are indebted to V. Baglin and O. B. Malyshev for valuable discussions. The measurements at ANKA were performed together with the ANKA machine group: I. Birkel, E. Huttel, A.-S. Müller, and P. Wesolowski. The authors would like to thank E. Huttel for useful discussions and A. Völker for technical support in setting up the H_2 experiment.

REFERENCES

[1] J. Chavanne, P. Elleaume, Proceedings of EPAC 2006, Edinburgh, Scotland 2006.

[2] S. Casalbuoni et al., *Phys. Rev. ST Accel. Beams* **9**, 010702 (2006).

[3] E. Levitchev et al., Proceedings of EPAC 2006, Edinburgh, Scotland 2006.

[4] J.A. Clarke et al., Proceedings of EPAC 2006, Edinburgh, Scotland 2006.

[5] http://ankaweb.fzk.de/

[6] S. Chouhan et al., Proceedings of PAC 2003, Portland, Oregon, USA 2003.

[7] SHI Cryogenics Group, http://www.apdcryogenics.com

[8] S. Casalbuoni et al., Proceedings of EPAC 2006, Edinburgh, Scotland 2006.

[9] E. Wallén, G. LeBlanc, *Cryogenics* **44**, 879 (2004).

[10] W. Chou and F. Ruggiero, LHC Project Note 2 (SL/AP), (1995).

[11] H. London, *Proc. Royal Society (London)* **A176**, 522 (1940); A.B. Pippard, *Proc. Royal Society (London)* **A191**, 385 (1947); G.E.H. Reuter and E.H. Sondheimer, *Proc. Royal Society (London)* **A195**, 336 (1948); R.G. Chambers, *Proc. Royal Society (London)* **A215**, 481 (1952).

[12] O. Gröbner, Proceedings of PAC 1997, Vancouver, Canada 1997.

[13] V. Baglin, B. Jenninger, LHC Project Report 721, 2004.

[14] http://cas.web.cern.ch/cas/Spain-2006/PDFs/Hilleret-1.pdf

[15] E. Wallén, *JVSTA* **14** (5), 2916 (1996).

[16] A. Kulikov et al., Proceedings of PAC 2001, Chicago, Illinois, USA 2001.

[17] A.-S. Müller et al., Proceedings of PAC 2005, Knoxville, Tennessee, USA 2005.

[18] F. Perez et al., Proceedings of PAC 2003, Portland, Oregon, USA 2003.

[19] A. Bernhard et al., Proceedings of Applied Superconductivity Conference, ASC 2006, Seattle, WA, USA, to appear in IEEE Transactions on Applied Superconductivity

[20] W.C. Turner, Proceedings of PAC 1993, Washington, D.C., USA 1993.

[21] I.R. Collins and O.B. Malyshev, LHC Project Report 274, 2001.

[22] S. Andersson et al., *Phys. Rev. B* **40**, 8146 (1989).

[23] V.V. Anashin et al., Vacuum **48** (7-9), 785 (1996).